Experimental and Theoretical Analysis of Photofragmentation of Au Nanoparticles by Picosecond Laser Radiation

ARTICLE *in* THE JOURNAL OF PHYSICAL CHEMISTRY C · FEBRUARY 2010

Impact Factor: 4.77 · DOI: 10.1021/jp908964t

4 AUTHORS, INCLUDING:

Francesco Giammanco
Università di Pisa
116 PUBLICATIONS **631** CITATIONS
SEE PROFILE

Emilia Giorgetti
Italian National Research Council
137 PUBLICATIONS **808** CITATIONS
SEE PROFILE

Anna Giusti
Charité Universitätsmedizin Berlin
26 PUBLICATIONS **347** CITATIONS
SEE PROFILE

Experimental and Theoretical Analysis of Photofragmentation of Au Nanoparticles by Picosecond Laser Radiation

Francesco Giammanco,[†] Emilia Giorgetti,*[,‡] Paolo Marsili,[†] and Anna Giusti[§,†]

Department of Physics "E. Fermi", University of Pisa, Largo Bruno Pontecorvo 3, Pisa, Italy, and INSTM and Istituto dei Sistemi Complessi, Consiglio Nazionale delle Ricerche, Via Madonna del Piano 10, Sesto Fiorentino (Firenze), Italy

Received: September 16, 2009; Revised Manuscript Received: January 20, 2010

This paper presents a novel model aimed at describing the basic phenomena that cause the fragmentation of a single Au nanoparticle (AuNP) by interaction with the second and the third harmonics of a Nd:YAG picosecond laser. In order to verify the model through a comparison with experimental results, we extended the single-AuNP fragmentation model to treat the macroscopic bleaching of a suspension of AuNPs. The sample of AuNPs is obtained by laser ablation in an aqueous solution of fifth generation ethylendiamine-core poly(amidoamine) (PAMAM-G5) with the fundamental wavelength of the same laser at 1064 nm. The dependence of photobleaching on the laser pulse energy at 355 and 532 nm is studied and hence compared with the theoretical model. In particular, we discuss the role of heating and the interplay among pure thermal processes, e.g., melting and evaporation, thermoionic emission, and photon-assisted ionization. We show that, although the AuNP temperature can overcome the evaporation threshold in our range of investigation, the experimental curves disagree with a process of fragmentation mainly driven by heating. Our results highlight the role of photon-assisted transitions in AuNP fragmentation and allow us to discuss different regimes of fragmentation at different fluences and intensities. Moreover, we show that PAMAM-G5 plays a crucial role in our experiments.

I. Introduction

Gold nanoparticles (AuNPs) produced in the form of colloidal suspensions by pulsed laser ablation of a metallic target are of great interest, especially for the fast developing fields of human biology and medicine, where nanoparticles seem suitable for drug delivery systems and in vivo and in situ diagnostics.[1] Laser-produced nanoparticles are envisaged to be particularly attractive for their purity, unlike those produced by chemical procedures. In this framework, laser-induced fragmentation is of particular interest as a means for growth limitation of colloids, which could otherwise prevent some applications. In the meanwhile, this effect can be exploited, once fully understood, to control the size and shape of preformed particles.[2−12] Moreover, from a more fundamental point of view, an appropriate model of fragmentation can help to improve the knowledge of laser−matter interactions in the nanoscale range.

Photofragmentation of metal nanoparticles has been extensively studied for more than 10 years. The experimental parameters are spread over a very wide range of fluences and laser pulse durations, which in turn determine the intensity range. A large variety of experimental methods have been employed basically to understand the NP response on a short time scale, comparable to or less than the laser pulse duration, to monitor the transient optical and structural properties during the interaction with a laser.[3,10,12−14] In addition, accurate measurements of physical−chemical properties, as melting point and thermal exchange with surrounding media, have elucidated the differences between NP and bulk values, as a function of NP radius.[15−19]

Two basic mechanisms have been identified as responsible for NP fragmentation under laser illumination, which can be schematically summarized as (i) thermal heating followed by evaporation and (ii) electron ejection, due to either thermoionic emission and/or photoionization, which leads NPs to fragment by Coulomb explosion. Laser intensity seems to be a good parameter to discriminate the dominance of one mechanism over another.

Concerning electron emission, we stress that, in some intermediate intensity regimes, as for instance that analyzed in ref 20, it is difficult to discriminate *a priori* between thermoionic and photoelectric ionization, since laser intensity could be enough to produce relevant thermoionic emission but negligible photoionization. Therefore, in many experiments in the nanosecond range,[10−12] although the main mechanism of NP fragmentation is due to electron ejection and not to evaporation, the photon-assisted processes seem to play a minor role compared with thermoionic emission.

Two experiments (refs 3 and 7) performed with picosecond pulses are of particular interest for a first survey of the peculiarities of this time/intensity regime. In ref 3, fragmentation of AgNPs with 355 nm pulses is observed and ascribed to a two-photon ionization, which brings the NP in a transient state, formed by charged clouds, before breaking into smaller clusters. The experiment was performed in Ag where the plasmon absorption coefficient at 355 nm, much higher than the corresponding one for Au, would in principle enhance the NP heating. The electron ejection is clearly monitored by the transient photobleaching of the plasmon band. Analogous transient photobleaching experiments were also performed with AuNPs

* Corresponding author. Tel.: +390555226691; fax: +390555226683; e-mail: emilia.giorgetti@fi.isc.cnr.it.
[†] University of Pisa.
[‡] Consiglio Nazionale delle Ricerche.
[§] Present address: Universite' Paris-Sud 11, Institut de Chimie Moléculaire et de Matériaux d'Orsay, UMR CNRS 8613, F-91405, Orsay, France.

10.1021/jp908964t
Published on Web 02/09/2010

by El Sayed and co-workers.[13] On the contrary, in ref 7 the authors observed the formation of a bimodal AuNP distribution under postirradiation of 40 nm uncapped AuNPs in water with picosecond pulses at 355 nm. They ascribed it to the formation around the particle of a vapor layer of gold, due to heating, followed by cooling and condensation into smaller NPs. The main difference between the previous experiments is, basically, the laser intensity, which in ref 3 is about 1 order of magnitude larger than that in ref 7. It seems to confirm the role of the intensity in defining the range where electron ejection processes, including thermoionic emission, would prevail over melting/evaporation.

In refs 2 and 21, we reported on an experimental analysis of the fragmentation caused by 532 or 355 nm ps pulses in a previously prepared colloidal suspension of AuNPs capped by fifth generation ethylendiamine-core poly(amidoamine) (PAMAM-G5), which is an efficient stabilizer for different metal NPs. We showed that irradiation with these wavelengths permits thorough bleaching of the plasmon band, transforming wine-red samples into transparent and clear suspensions with no evidence of gold precipitation, even after several months. This suggests that, in both cases, the existing nanoparticles are broken into subnanometer fragments, whose dimensions are so small that the plasmonic band is completely damped. Such fragments do not recombine into nanoparticles or into a precipitate, because they can be trapped and stabilized by PAMAM-G5 molecules. In our experiments, the fingerprint of the photofragmentation effect was the growth of a new band, which appeared in the absorption spectra of the suspensions and which we attributed to a charge transfer between gold cations trapped within the PAMAM cavities and the PAMAM molecule itself.[2,22] More recently, by Mie fitting of the absorption spectra of PAMAM-G5-capped AuNPs suspensions before and after irradiation with 532 or 355 nm pulses, we showed that the bleaching of the plasmon is also accompanied by the growth of the absorption in the blue region of the spectrum.[23] This absorption, assigned to interband transitions of gold, is clearly related to the efficient formation of subnanometer clusters. In this sense, PAMAM-G5 plays a key role in such fragmentation experiments, because it freezes all the fragmentation byproduct, i.e., Au cations and subnanometer clusters, and gives a shot-by-shot picture of what happens during laser irradiation.

In ref 2, we gave a first explanation of the nonlinearity of the fragmentation process with 532 nm pulses in terms of a 2-photon extraction of electrons from the nanoparticles, which became positively charged, unstable, and eventually underwent a Coulomb explosion when the "fissility" became greater than 1.[10,24] Indeed, although the workfunction of bulk gold is 5.1 eV, both the small dimensions of the nanoparticles and the chemisorption of an organic compound on their surface are compatible with a reduction of the order of 8−10%, which leads to a value below that corresponding to a couple of photons at 532 nm, namely, 4.64 eV.[20,25,26] Moreover, this value is also consistent with ionization running from low-index crystalline planes of gold.[20,26]

The ambitious purpose of this paper is to build up a theoretical model that, besides explaining our results, could be of some help to quantitatively analyze the role of the envisaged processes under different experimental conditions and to justify some of the apparently contradictory results reported in the literature.

In Section III(a), we discuss some relevant findings, which suggested to us that the explanation of the macroscopic evolution of the plasmon band of our samples could not be ascribed to simple evaporation. It helps to state the basis of the overall model, which is extensively discussed in Sections III(b), (c) and (d). Comparison with our experimental results and some insights of the model are given in Section IV, then followed by a discussion on relevant physical aspects pertaining to different experimental conditions.

II. Experimental Methods

We prepared AuNPs suspensions in solutions of PAMAM-G5 in water. The solutions were 3.8 mM in reference to superficial amino groups and were obtained by dilution of a 6.67% aqueous solution of amino-terminated PAMAM-G5 from Dendritech with ultra pure water (18.2 MΩ·cm @ 25 °C). According to tabulated values provided by the producer, PAMAM-G5 is a monodisperse compound, having a molecular diameter of 5.4 nm.

The ablation was performed by irradiating a gold target (purchased from Goodfellow) with the fundamental wavelength (1064 nm) of a mode-locked Nd:YAG laser (EKSPLA PL2143A: rep. rate 10 Hz, pulse width 25 ps) with 15 mJ pulse energy. The infrared wavelength was chosen because it does not cause any damage either to nanoparticles or to stabilizing molecules, as noticed in ref 2. The focusing conditions of the laser beam were maintained constant, and the diameter of the laser spot on the target was fixed at 1.4 mm. The target was placed in a 1 cm × 1 cm quartz cuvette and was kept 2 cm in front of the focal plane of the laser beam. In each ablation we used 2 mL of stabilizing solution. During the preparation, we recorded the absorption spectrum (see below) in order to produce samples with the same plasmon peak absorbance, i.e. 1.1 ± 0.1, and shape (Figure 1a).

The particle mean diameter and dispersion were determined by transmission electron microscopy (TEM) analysis. We found an average value of the radius $R_{NP} = 1.75$ nm and a standard deviation $\sigma_{NP} = 0.75$ nm (Figure 1b). Once the size-distribution is known, the initial density D_{NPo} of AuNPs can be calculated by fitting the absorption spectrum of the suspension with Mie's cross section in the dipole approximation. We obtained $D_{NPo} = 6.5 \times 10^{13}$ NP/cm.[3,23,27]

We post irradiated the obtained suspensions by using the third harmonic (355 nm, pulse width 15 ps) or the second harmonic (532 nm, pulse width 20 ps) from the same laser. The focusing conditions of the laser beam were maintained constant and were the same as during ablation. During the bleaching, the laser beam illuminates a truncated cone in a 1 cm^2 base cell filled with 1 or 2 cc of suspension. The height of the cone (z axis) depends on the amount of suspension, i.e., it can be 1 or 2 cm.

The ablation process and the subsequent photofragmentation of the nanoparticles were monitored by measuring in situ the visible spectra with an Ocean Optics fiber spectrophotometer and an Ocean Optics source equipped with deuterium and tungsten lamps. The sampling beam was perpendicular to the picosecond laser beam and crossed the quartz cuvette 0.3 cm above the bottom of the cell. The spectra were acquired in sequence every preselected number of shots and then elaborated to give the in situ absorbance versus wavelength by an appropriate LabView program, which subtracts from each spectrum the reference spectrum pertaining to a PAMAM-G5/water solution without the colloid. Generally, a significant variation of the absorbance was observed every 200−500 shots, depending on the laser pulse energy. In addition, the program also allowed us to record in a separate file the absorbance versus laser shots at preselected wavelengths. The latter option is a convenient reference for our previous analysis at fixed frequency.[2] In particular, we evaluate the strength of bleaching at

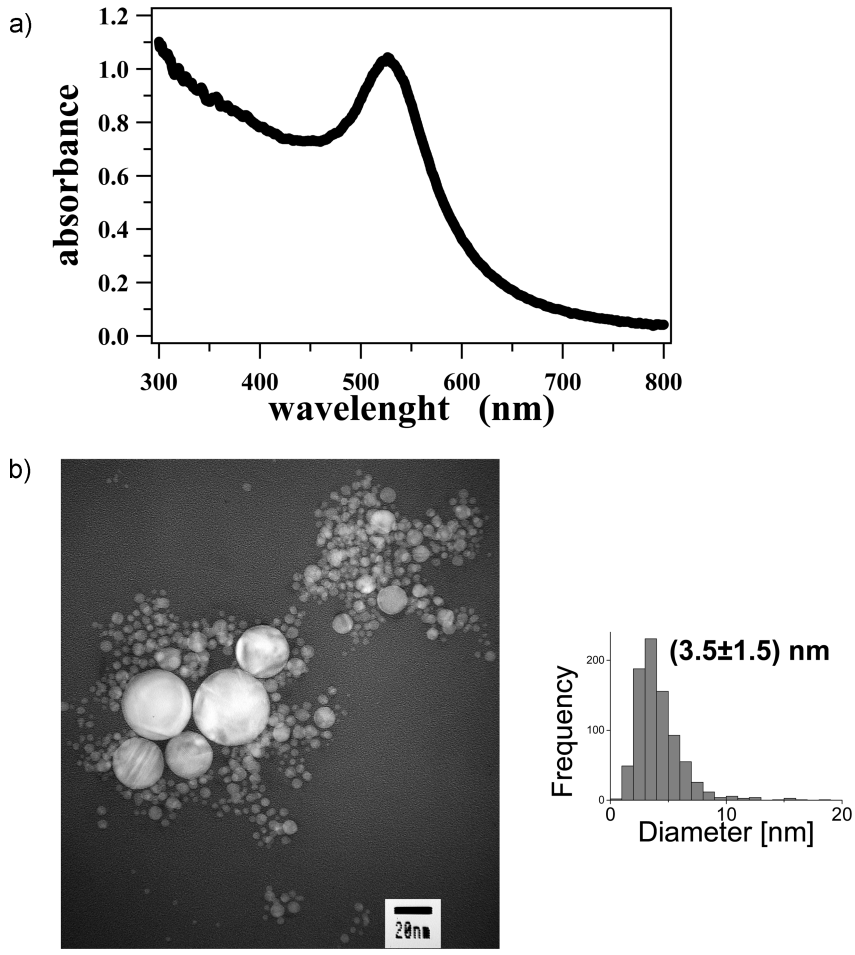

Figure 1. (a) UV−vis absorption spectrum and (b) TEM image with statistical distribution of particle size of a suspension of PAMAM-G5-capped AuNPs obtained by ablation with 15 mJ pulses at 1064 nm.

different energies, which we assume as a definition of the decay constant τ_{blc}, by measuring the inverse of the number of shots required to reduce the initial plasmon band peak by $1/e$.

Samples for TEM inspection were obtained by dipping copper grids in the suspensions, and the images were recorded with a HRTEM JEOL2010, 200 KV.

III. Theoretical Model

In this section, we build up a model that includes all the processes that can be responsible for photofragmentation of AuNPs, namely, evaporation caused by heating above the melting point and electron ejection with subsequent size reduction or explosion of the AuNPs.

III(a) Preliminary Discussion. Figure 2a shows the evolution of the plasmon band during the bleaching of a suspension of PAMAM-G5-capped AuNPs with 15 mJ at 532 nm. As a comparison, Figure 2b illustrates the completely different process of plasmon bleaching observed in the case of uncapped AuNPs produced and postirradiated in pure water in the same conditions as those of Figure 2a. The inset of this figure also shows the 14 h time evolution of the plasmon band after switch-off of the 532 nm beam. Eventually, Figure 2c reports the evolution of the plasmon maximum versus the number of laser shots in both cases.

While bleaching of capped AuNPs proceeds monotonically according to an exponential decay with $\tau_{blc} = 3 \times 10^{-4}$, in the case of uncapped AuNPs, after an initial decrease similar to that of the capped ones, the plasmon peak suddenly turns back close to its initial value and finally decays with $\tau_{blc} = 4 \times 10^{-5}$. The comparison of the spectra of Figure 2a,b allows a better understanding of the differences. The spectra of Figure 2a are *quasi* self-similar and show a monotonic decay of the plasmon peak, which maintains its spectral position. Neither near-infrared absorption nor precipitation were observed with PAMAM-capped AuNPs. In contrast, the spectra of Figure 2b show that initially fragmented uncapped AuNPs reaggregate (green and blue curves in Figure 2b), form complex structures, clearly tagged by the growth of a broad absorption band in the near-infrared region (blue and light-blue spectra in the inset of Figure 2b), and eventually precipitate (yellow and navy blue spectra in the inset of Figure 2b). As a matter of facts, reaggregation of uncapped fragments and subsequent precipitation can be an indirect proof of the role of electron ejection. Indeed, they were attributed to a positive charging of irradiated NPs, which, under diffusion outside the illumination cone, can easily fuse with nonirradiated, negatively charged ones.[28,29]

Besides being different in its evolution and final products, the overall bleaching process for uncapped AuNPs requires a much larger number of shots than for PAMAM capped ones. All these findings suggest that the type of capping, beyond all the other experimental parameters, such as laser wavelength, fluence, and pulse width, can also play a fundamental role in determining the relative importance of the different physical mechanisms involved in the process.

III(b) Heating and Evaporation of a Single AuNP. Heating and cooling of a single AuNP has been extensively analyzed in

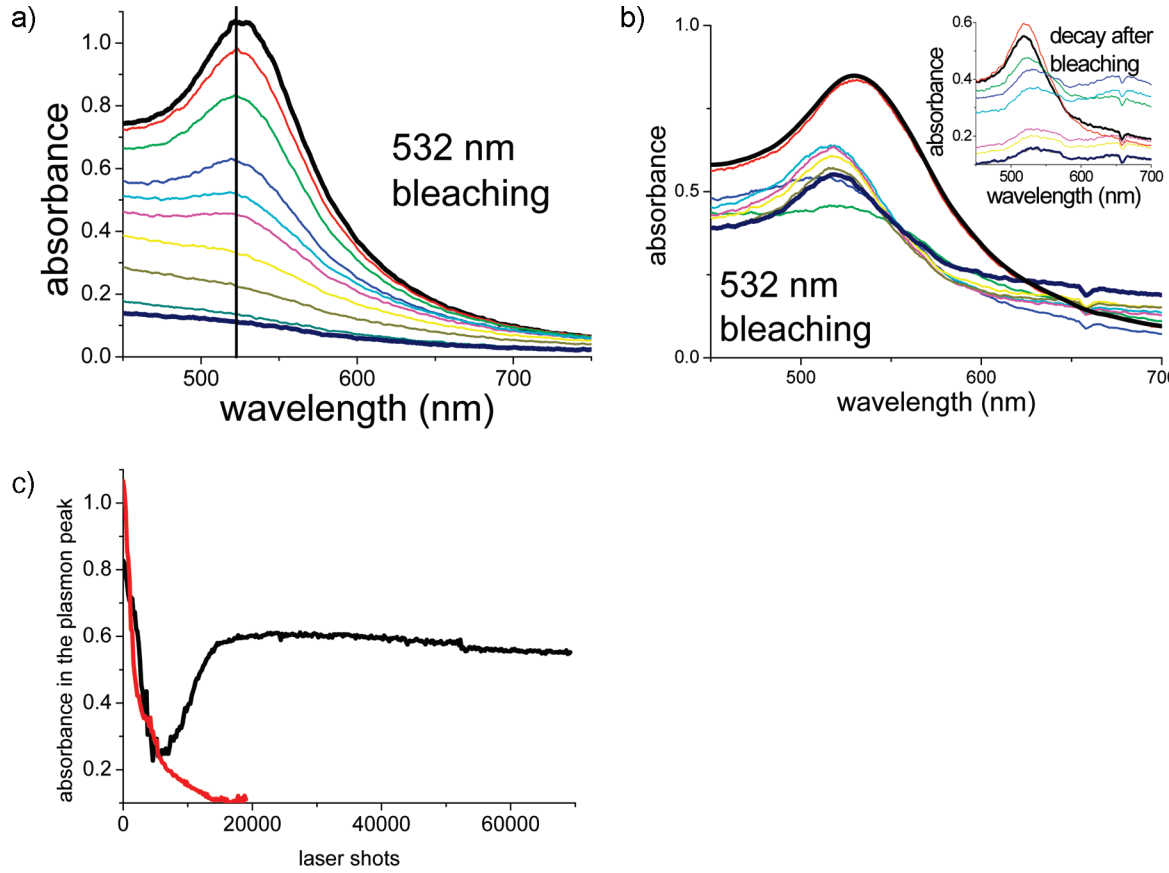

Figure 2. Evolution of the plasmon band during the bleaching with 15 mJ at 532 nm of a suspension of PAMAM-G5-capped (a), or uncapped (b) AuNPs. The inset of (b) shows the 14 h time evolution of the plasmon band after switch-off of the 532 nm beam. In each case, thick black and thick navy curves represent the initial and final spectra, respectively. (c) evolution of the plasmon maximum versus the number of laser shots in the case of PAMAM-G5-capped (red curve) and uncapped (black curve) AuNPs.

the literature, and basic equations have been well stated (see, for instance, ref 20). They describe the heating of a AuNP caused by the laser energy absorbed by the conduction electrons and subsequently transferred first to the lattice, through electron−phonon collisions, and then to the surrounding medium by thermal diffusion. Assuming uniform T_e and T_l inside the AuNP, i.e., the electron and lattice temperatures, respectively, the coupled heat equations read[20]

$$\gamma T_e \frac{dT_e}{dt} = -G(T_e - T_l) + P_L(t) \quad (1)$$

$$C_l \frac{dT_l}{dt} = G(T_e - T_l) - P_{lM}(t) \quad (2)$$

where γT_e, C_l, and G are the electronic and lattice heat capacities and the electron−phonon coupling constant, respectively. $P_L(t)$ is the energy-exchange with the laser pulse, while $P_{lM}(t)$ represents the energy-exchange with the surrounding medium.

It is worthwhile to express all constants in eqs 1 and 2 in units of unitary volume to emphasize the dependence on the AuNP radius R_{NP}. The energy-exchange with the laser pulse is given by $P_{L(t)} = [\sigma_{Mie}/(4/3)\pi R_{NP}^3]I_L(t)$, where σ_{Mie} is Mie's absorption cross section[13] and $I_L(t)$ is the laser intensity.

The energy dissipation of AuNPs of different sizes (4−50 nm) in water has been measured accurately by Hu and Hartland with pump−probe spectroscopy.[17] They found that cooling does not follow an exponential decay, but it can be reasonably approximated by a stretched exponential such as $\exp[-(t/\tau)^{0.7}]$. The decay constant τ turned out to be proportional to R_{NP}^2. For $R_{NP} = 2.5$ nm, they measured $\tau \approx 10 \pm 5$ ps,[17] which in turn leads to a value of 7 ps for the average radius of our particles. Moreover, the authors found the dissipation rate to be independent of the initial temperature of the AuNP. Consequently, although in our conditions we expect that the lattice thermal excursion be much larger than that used in ref 17, we can make the same hypothesis. On this basis, we insert in eq 2 $P_{lM}(t) = 0.3(T_l - T_M)/(\tau)$ for $t < \tau$ and $P_{lM}(t) = 0.3(T_l - T_M)/(t^{0.3}\tau^{0.7})$ for $t \geq \tau$. Then we add to the system of eqs 1 and 2 an equation for T_M, which is the ambient temperature around a AuNP, in the form

$$\frac{\partial T_M}{\partial t} = P_{lM}(t) \quad (3)$$

An important issue is proper choice of the value of the coefficients γ, G, and C_l. The coefficients γ and G can be considered constant for $T_e \leq 0.3$ eV, their values being $\gamma = 63$ J/m^3·K^2, and $G = 2.5 \times 10^{16}$ W/m^3·K, respectively.[20] However, since in our range of energy variation T_e can become far greater than 0.3 eV, we have to consider the dependence of γ and G on T_e. According to ref 20, γ and G are enhanced by factors of about 2 and 6, respectively, as the electron temperature rises from 0.3 to 1 eV, and then saturate. More recently, the electron capacity C_e ($C_e = \gamma T_e$), the electron−phonon coupling G and the chemical potential μ have been recalculated as a function of T_e including the contribution of d electrons, which is peculiar

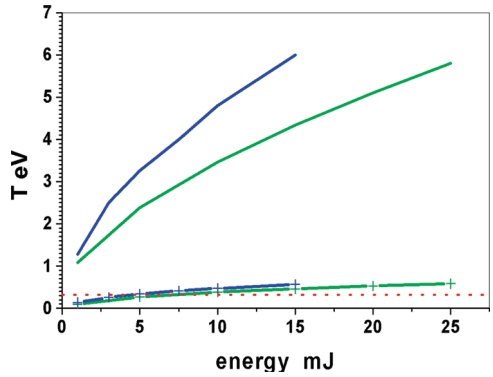

Figure 3. Calculated maximum values of T_e (solid lines) and T_l (dashed lines) reached during a single laser shot versus the laser energy. Violet and green colors represent results at 355 and 532 nm, respectively. The dotted red line approximately indicates the evaporation limit.

of Au.[30] The calculation has been performed over a large range of T_e and the results are available on line as data files,[30] which we used for calculating T_e and T_l. Compared with ref 20, both C_e and G are enhanced up to saturation by factors of about 3.5 and 10, respectively. Concerning the lattice heat capacity, we assumed the bulk value $C_l = 2.5 \times 10^6$ J/m^3·K. Even if many thermodynamic properties change with the size of a AuNP, nowadays there is no evidence to suspect a dramatic change of C_l at temperatures much above the bulk Debye temperature (170 K), which could justify a strong reduction of AuNP heating. In addition, recent works demonstrate that Debye temperature exhibits a reduction on the nanoscale.[31]

The solutions of the system of eqs 1−3 are shown in Figure 3, which reports the results of our calculations, that is, the maximum values of T_e (solid lines) and T_l (dashed lines) reached during a single laser shot versus the laser energy. Violet and green colors represent results at 355 and 532 nm, respectively. The straight line approximately indicates the evaporation limit.

On the basis of Figure 3, it seems difficult to exclude *a priori* evaporation as the main process of AuNP fragmentation in our range of fluence, i.e., 0.2−1.5 J/cm^2 and 0.5−2 mJ/cm^2 for 355 and 532 nm, respectively. Then, we include this effect in the complete model among the possible mechanisms of fragmentation.

Furthermore, it must be taken into account that evaporation does not necessarily destroy an NP in a single laser shot. For example, according to ref 7, a fluence of 0.43 J/cm^2 causes an average reduction of particle volume η around 0.1. Since our experimental fluences were up to 5 times larger, following a simple linear extrapolation, we assumed $\eta = 0.5$ at the top end of our range of fluence. To include this effect into the model, we assumed that, at the end of each laser shot, the number of atoms in the AuNP is reduced by a factor $(1 - \eta)$, if the lattice temperature has overcome the evaporation point, i.e., 0.3 eV.[7] This condition is then inserted in the overall scheme of bleaching of the entire suspension (see Section III(d)).

III(c) Electron Ejection from a Single AuNP. Basically, ionization can be caused by a purely thermal effect, i.e., thermoionic emission, by multiphoton transitions from Fermi level, which do not require any heating to populate the lowest state of transition, and by a mix of them. A third mechanism includes all the photon-assisted transitions to continuum whose initial states lie in between the Fermi level and the continuum, namely transitions from levels that are populated through heating of the conduction electrons of a AuNP. They are single photon when the initial electron energy E lies within the interval $W_F - h\nu_L \le E \le W_F$, where W_F is the work function, and $h\nu_L$ is the photon energy, and two-photon when $W_F - 2h\nu_L \le E \le W_F - h\nu_L$ or in general, depending on the work function, n photons when $W_F - nh\nu_L \le E \le W_F - (n-1)h\nu_L$. Depending on the value of the work function W_F, in principle the scheme described below can be extended to any n-order.

In order to calculate the contribution of each process to the ionization of a single AuNP and hence to extend the result to the ensemble of particles in the suspension, we made some assumptions.

First, we assumed that the Fermi distribution function $f(E) = 1/(1 + \exp[(E - \mu)/kT_e])$ holds true independently of R_{NP}, at least until $R_{NP} \ge 0.5$ nm, i.e., the lowest value required to have plasmon resonance. μ is the chemical potential coincident with the Fermi energy E_F for $T_e \approx 0$.

Therefore, the rate of ionization due to thermoionic emission reads[20]

$$\left(\frac{dN_e}{dt}\right)_{therm} = \frac{N_{eT}(t)}{\tau_{ee}} \frac{1}{f(0)} \left(\frac{df(E)}{dE}\right)_{\mu=W_F} = \frac{N_{eT}(t)}{\tau_{ee}} \frac{1}{1 + e^{-\mu/kT_e}} \frac{e^{W_F/kT_e}}{(1 + e^{W_F/kT_e})^2} \quad (4)$$

where τ_{ee} is the electron−electron collision time, $\tau_{ee} \approx 2 \times 10^{-14}$ s,[32] and $N_{eT}(t)$ is the total electron density in the conduction band, which decreases in time because of ionization. According to ref 30, the usual Sommerfeld expansion for μ, $\mu_{Sommer} = E_F[1 - (\pi^2/12)(k_B T_e/E_F)^2]$, does not hold in Au for $T_e > 0.3$ eV, since the contribution of d electrons cannot be neglected. Then, as for C_e and G, we made use of datafiles provided online by the authors.[30] It is worth noting that calculations show an increase of μ as T_e increases, while Sommerfeld expansion predicts a decrease, e.g., at $T_e = 3$ eV, $\mu \approx 7.5$ eV against $\mu_{Sommer} \approx 5.2$ eV.

The second relevant approximation deals with the rate of photon-assisted transitions, i.e., 1, 2, or n photons. As already observed, 1-photon and 2-photon transitions affect all electrons whose energy lies within the energy interval $W_F - h\nu_L \le E \le W_F$ and within $W_F - 2h\nu_L \le E \le W_F - h\nu_L$, respectively. Hence, the probability of transition is expected to change over the interval related to the selected transition. Generally speaking, the rate of electron ejection due to an n-order photon transition can be expressed as

$$\left(\frac{dN_e}{dt}\right)_{nph} = \int_{E_{min}}^{E_{max}} \alpha_n(E) I_L^n N_{eT}(t) dg(E) \quad (5)$$

where $\alpha_n(E)$ is the probability of transition from an energy state E within the range $E_{min} = W_F - nh\nu_L \le E \le E_{max} = W_F - (n-1)h\nu_L$, and $dg(E)$ represents the differential density of states given by $dg(E) = 9[4\pi(2m)^{3/2}/h^3][E^{1/2}/(1 + \exp[(E - \mu)/kT_e])]dE$ where h and m are the Planck constant and the electron mass, respectively.

Since data and/or theoretical estimations of $\alpha_n(E)$ are very poor or do not exist at all, we use an approximate formula which allows the calculation of the saturation intensity for a n-order nonresonant ionization, given the ionization potential (W_F) and the laser pulse duration.[33] The saturation intensity, i.e., the intensity producing a degree of ionization of about 0.63, is related to the probability of ionization by $\alpha_n(E) = (n/\pi)^{1/2}[1/\tau_L P_{sat}^n(E)]$ where τ_L is the half width at half-maximum (HWHM) laser pulse duration. From ref 33, the saturation intensity in practical units reads

$$P_{sat}^{n}(E) = \frac{1.38 \times 10^{12} \Delta W_{eV}{}^{3}}{\left[1.1 \times 10^{3} \Delta W_{eV} \tau_{ps} (2n+1)^{(2n+1)} e^{-(2n+1)} B\left(\frac{1}{2}, n\right)\right]^{1/n}} \text{ W/cm}^2 \quad (6)$$

where $\Delta W_{eV} = W_F - E$ is the energy gap required to ionize electrons of energy E, and is expressed in eV, τ_{ps} is the laser pulse duration in picosecond units, and $B(1/2, n) = \int_0^1 x^{-1/2}(1-x)^{n-1}dx$.

Equation 6 works very well to calculate the saturation intensity for n-order transitions in atomic collisionless gases, and it can be easily handled to calculate eq 5, since it contains an explicit dependence on the energy gap ΔW_{eV}, which makes the numerical evaluation of the integral easier. Equation 6 also defines the maximum n-order that can give significant contribution to ionization, e.g., an expected $n = 3$ transition on the basis of $nh\nu > W_F$ does not take place if the laser power is much less than $P_{sat}{}^3$.

In conclusion, the total number of electrons in the conduction band decreases within a laser pulse according to

$$\frac{dN_{eT}(t)}{dt} = -\left(\frac{dN_e}{dt}\right)_{therm} - \sum_{jph=1}^{n} \left(\frac{dN_e}{dt}\right)_{jph} \quad (7)$$

where the first term refers to thermoionic ionization and the second term refers to photon-assisted processes, each of them given in the form of eq 5. Summation extends to the lowest photon order required to overcome W_F.

To calculate eq 7, it is important to choose the proper value for W_F. On the basis of the definition of the work function, i.e., the work done against the force acting on an electron emerging from the surface of a metal,[34] one can expect a dramatic increase as long as the ionization develops, independently of its initial value.

Usually, for a single electron, assuming a planar metallic surface at zero potential, the work function is given by $W_F = e^2/16\pi\varepsilon_o d_{mfp}$, where e is the elementary charge and d_{mfp} is of the order of the electron mean free path in the metal lattice. With $d_{mfp} \approx 8 \times 10^{-11}$ m, we obtain the bulk value of $W_F = 5.1$ eV. In analogy with this derivation, we now consider the problem of the work required to remove one electron from an isolated, conducting sphere of radius R_{NP} and charge Q. The problem is solved in ref 34 by the method of images. The work to displace to infinity one electron is given by $W = (1/4\pi\varepsilon_o)[Qe/y_o + e^2 R_{NP}{}^3/2y_o(y_o{}^2 - R_{NP}{}^2)]$ where y_o gives the position of image charges inside the sphere. Taking $y_o = R_{NP} + d_{mfp}$, with $d_{mfp} \ll R_{NP}$, and after some rearrangement we find

$$W_F = \frac{1}{4\pi\varepsilon_o}\left(\frac{Qe}{R_{NP}} + \frac{e^2}{4d_{mfp}}\right) \quad (8)$$

Expressing the energy in electron volts, R_{NP} in nanometers, and Q in terms of the number of ejected electrons N_e, eq 8 reads $W_F = W_{Fo} + (1.56/R_{NP})(N_e - 1)$, where W_{Fo} is the usual definition of W_F for an uncharged conductor. Also W_{Fo} undergoes some weak changes during heating and ionization. According to ref 35, W_{Fo} is proportional to $N_e{}^{1/2}$ and to $\mu^{-1/2}$, i.e., $W_{Fo} = W_{Fi}(E_F/\mu)^{1/2}(N_e/N_o)^{1/2}$. N_o is the initial number of atoms in the AuNP, i.e., $N_o = (R_{NP}/R_{At})^3$, where R_{At} is the half distance among atoms in the lattice, i.e., for Au, $R_{At} = 0.15$ nm. It is evident that the effect of an increasing attractive force as electron ejection develops is less important for larger AuNPs. In this respect, owing to the small average size, our experiments are less favored, if compared with many others available in the literature. It is worth noting that eq 8 represents an overestimation of the effect of the negative space charge accumulating around a NP as the ionization proceeds. In fact, we assume that all the negative charge is imaged over the NP, neglecting that (a) the kinetic energy of ejected electrons spans from almost zero to about the photon energy (see above); (b) as the negative charge accumulates, the cloud expands because of Coulomb repulsion; and (c) any effect due to electron scavengers can reduce the negative charge. A more realistic modeling of the space charge surrounding a AuNP is presently underway. For the present purposes, the assumption of a fully imaged negative charge can help to emphasize the role of electron ejection in the worst case.

As the ionization goes on, a positive charge Q continues to accumulate on the NP during the laser pulse and eventually prevents further ionization. Nevertheless, the AuNP becomes progressively unstable as the positive charge accumulates until the fissility parameter overcomes 1, which, for gold, corresponds to[10,24]

$$Q \geq \sqrt{N_o/0.9} \quad (9)$$

When the positive Q charge satisfies eq 9, the particle is depleted by an amount Q of atoms and recovers its electrical neutrality. Therefore, at the beginning of the following laser pulse, the initial conditions are restored, in particular $W_F = W_{Fi}$. If the condition expressed by eq 9 is not matched, W_F maintains the final value achieved during the previous laser pulse. A direct evaluation of the positive charge left by electron ejection can be done by taking into account that the initial electron density in the conduction band is related to the AuNP radius by the relationship $N_{eT}(0) = N_o/(4/3)\pi R_{NP}{}^3$, and hence by multiplication of eqs 4, 5, and 7 by the AuNP volume.

III(d) Extension to an Ensemble of AuNPs in Suspension. The equation system 1−5 describes the interaction of the laser pulse with a single AuNP. Since we detect the whole bleaching process of many AuNPs in suspension through the decay of plasmon absorption, we now have to extend the model to the ensemble of AuNPs and, eventually, calculate the absorption curve at the geometrical detection position in the sample.

From Mie's cross section, the density of nanoparticles and the focusing parameters, it is possible to calculate the absorption spectrum of a suspension versus number of laser shots at the sampling position.

Because of the small size of our AuNPs, the dipole approximation holds true, and then Mie's cross section reads[27]

$$\sigma_{Mie}(\omega, R_{NP}) = 9\frac{\omega}{c}\varepsilon_M{}^{3/2}\frac{4\pi R_{NP}{}^3}{3}\frac{\varepsilon_{IM}(\omega, R_{NP})}{[\varepsilon_{RE}(\omega, R_{NP}) + 2\varepsilon_M]^2 + \varepsilon_{IM}(\omega, R_{NP})^2} \quad (10)$$

The subscripts RE and IM refer to the real and imaginary part of the dielectric constant, which is corrected with respect to the bulk value by size-dependent dumping terms, namely,

$$\varepsilon_{RE}(\omega, R_{NP}) = \varepsilon_{RE\infty}(\omega, R_{NP}) + \omega_p{}^2\left(\frac{1}{\omega^2 + \Gamma_\infty{}^2} - \frac{1}{\omega^2 + \Gamma(R_{NP})^2}\right) \quad (11)$$

$$\varepsilon_{IM}(\omega, R_{NP}) = \varepsilon_{IM\infty}(\omega, R_{NP}) + \frac{\omega_p{}^2}{\omega}\left(\frac{\Gamma(R_{NP})}{\omega^2 + \Gamma(R_{NP})^2} - \frac{\Gamma_\infty}{\omega^2 + \Gamma_\infty{}^2}\right) \quad (12)$$

The subscript ∞ refers to the bulk values, $\Gamma(R_{NP})$ is the size-dependent relaxation frequency given by

$$\Gamma(R_{NP}) = \Gamma_\infty + \Psi\frac{u_F}{R_{NP}} \quad (13)$$

u_F is the Fermi velocity, Ψ is a coefficient on the order of 1,[27] and ε_M is the real dielectric constant of the surrounding medium. Hence, the energy exchange of the NP with the laser pulse $P_L(t)$ depends on the size only through the values of the dielectric constant $\varepsilon(\omega,R_{NP})$.

The laser absorption coefficient is given by

$$A(t) = D_{NP}(t)\int_0^\infty G(R,t)\sigma_{Mie}(\omega_L, R)\mathrm{d}R \quad (14)$$

where $G(R,t)$ represents the normalized size-distribution function of the AuNPs. We introduced a simplification in eq 14, since we assumed that the diffusion time is shorter than the inverse of the laser repetition rate. Under this assumption (see Section IV), the AuNP density and its distribution turn out to be uniform, and the z dependence in eq 14 is eliminated. Hence, the laser intensity along the focusing cone reads $I(z,t) = I(0,t)e^{-A(t)z}$. Note that, in principle, the initial shape of $G(R,t)$ can be modified during the bleaching. Then, the model was adapted to account for the effective size distribution of AuNPs. Nevertheless, even if smaller particles are expected to bleach faster, calculations show that the size distribution does not depart significantly from the initial one as shown by the spectral evolution of Figure 2a. Actually, as long as average particle radius decreases, the absorbed energy decreases as well. This lowers the electron temperature and slows the ionization. On the other side of the distribution, AuNPs larger than the average radius heat faster. Considering their relative weight on the distribution, it turns out that the evolution of the distribution is substantially *quasi* self-similar.

$A(t)$ rules the bleaching process along a focusing cone within the sample. Since both 355 and 532 nm wavelengths are absorbed by the suspension, the bleaching proceeds layer-by-layer, especially in the case of very dense samples. To evaluate it, we first determine a layer thickness dz so that laser intensity can be considered constant inside a volume $\mathrm{d}V(z) = \pi\rho_s{}^2(z)\mathrm{d}z$, where $\rho_s(z)$ is the laser spot size at position z. Then, we assume that all the AuNPs in such elementary volume are fully bleached when a single AuNP in the same conditions is bleached. Depending on the initial laser intensity and AuNPs density D_{NPo}, one or more or the whole focusing volumes can be bleached after the same number of shots. When a single AuNP in one or more elementary volumes is thoroughly bleached, iteration starts again with the density of AuNPs reduced by a factor $D_{NP}/D_{NPo} = 1 - [\sum \mathrm{d}V(z)/V_o]$, where V_o is the total volume of the suspension. Summation extends to the bleached elementary volumes. The previous assumption is correct, provided that AuNP diffusion time is short enough to refill the bleached volume(s) with a fresh amount of AuNPs. Although this condition is not always fulfilled in our range of investigation (see below), especially for higher energies, nevertheless, it barely affects the general trend given by the model.

To compare the theoretical model with the experimental results, the program calculates the decay of the maximum plasmon absorption versus the number of laser shots. In analogy with the experimental procedure (see Section II), we assumed as the theoretical decay constant the inverse of the number of shots required to reduce the initial value of the maximum plasmon absorption to 1/e.

IV. Comparison with Experimental Results and Discussion

As stated in Section II, we monitored the bleaching process by measuring the inverse of laser shots required to reduce the initial plasmon maximum absorption to 1/e, which we call the decay rate τ_{blc}. We assumed this definition in ref 2 since the decay of the plasmon maximum was found to agree well with an exponential law such as $\exp(-\tau_{blc}N_{shot})$. Here, we adopt the same definition, and we use the evolution of the overall spectrum as a reference. Theoretical calculations of the decay of the maximum plasmon absorption also gave an exponential law, thus confirming the validity of the previous assumption.

We observed that the experimental value of τ_{blc} showed noticeable fluctuations for laser energies above 5 mJ, for 355 nm and 10 mJ, for 532 nm. Initially, we ascribed that to the relevant role of thermal diffusion. In principle, as the bleaching goes faster, the refilling of the laser focusing cone should be fast enough to ensure an almost uniform density in between two subsequent laser shots. This is related to the incoming AuNP flux in the interaction volume. Moreover, there is an outgoing flux, which can be enhanced as the laser energy increases. In practice, there is an energy transfer from the AuNPs lattice thermal energy to the surrounding medium, which increases by absorption of laser energy (eq 3). The enhanced temperature of the medium, i.e., water in our case, leads to a reduction of the viscosity and hence increases the outgoing diffusion. Both effects tend to create thermal gradients and hence turbulent nonuniform suspensions. In principle, one can expect that stirring and thermal stabilization of the suspensions would mitigate the influence of diffusion. Actually, we obtained only marginal benefits by applying these methods, especially in the high-energy range of investigation. This suggested that the influence of these phenomena could take place on a time scale that is shorter than that of the gradient smoothing due to the thermomechanical action. On the other hand, on the basis of the theoretical model, it could also depend on the interference between vaporization and ionization, one prevailing on the other one, depending on the reproducibility of the experimental conditions, in particular the laser focusing, which controls the intensity level along the illuminated cone. A detailed analysis of this phenomenon is presently in progress. However, in the present work, to minimize the effect of the scattering of data due to fluctuations, we repeated each series of measurements three times for both wavelengths.

As described in Section III, our model accounts for both evaporation and electron ejection as causes of AuNP fragmentation. According to this model, if the lattice temperature overcomes the evaporation limit, i.e., 0.3 eV, electron ejection stops, and the AuNP undergoes a volume fractional loss η. For both wavelengths, we assumed a linear dependence of η on the

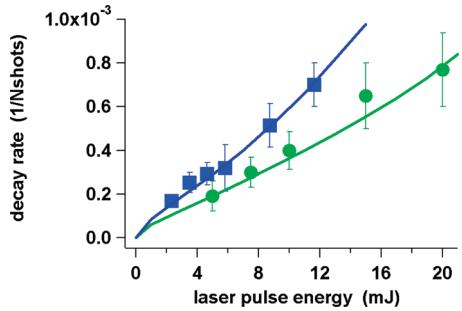

Figure 4. Comparison of theoretical dependence (continuous lines) and experimental data (dots) at 532 nm (green) and 355 nm (violet). Volume of bleached suspension 1 cm^3. $W_F = 4.6$ eV.

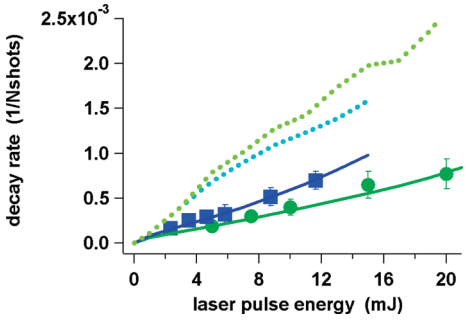

Figure 5. Theoretical dependences of the decay rate due to evaporation versus pulse energy (dotted lines) at 532 nm (acid green) and 355 nm (light-blue). For the convenience of the reader, the theoretical and experimental data of Figure 4 are also reported as references.

laser energy, starting from the minimum value $\eta = 0.1$ for 5 mJ pulses[7] (see Section III(b)). On the contrary, if the ejected charge Q matches the condition of eq 9, the ionization prevails.

When running our model, we assumed $W_{Fi} = 4.6$ eV. We have tested lower values or the bulk one, but we have not found this choice to be critical, W_F being essentially dominated by the image charge contribution (eq 8).

Figure 4 shows the comparison between our theoretical model and the experimental data for the bleaching of 1 cc of suspension with 355 (violet squares and solid line) and 532 (green circles and solid line) nm. Dots in Figure 4 are average values, and error bars correspond to the standard deviation. Compared with previous measurements,[2,21] we extended the energy range to 20 mJ for 532 nm and 12 mJ for 355 nm, which correspond to the maximum harmonic conversion of our crystals. The theoretical curves of Figure 4 represent an *ab initio* calculation where the input parameters account for colloid concentration and statistical size distribution of NPs, geometry of laser focusing, laser pulse energy, duration and wavelength, as well as the material parameters such as dielectric constant and work function. The agreement between experiment and theory is excellent, with no need of any renormalization coefficient.

Figure 5 shows the results of the model excluding the ionization and assuming that evaporation is the only cause of AuNPs bleaching. They are represented by acid green (532 nm) and light-blue (355 nm) dotted curves. The figure also reports the complete fittings of Figure 4 as a reference. It is clearly evident that, below 3 mJ, the dotted and continuous curves are barely coincident and that, in our conditions, the ionization prevails above 3 mJ. The differences are not so marked, as far as the shape of the curves is concerned. In particular, by taking into account the experimental errors and by properly renormalizing the curves, a certain degree of agreement between theory and experiment could be achieved also by assuming a fully thermal process. However, the output of our full model gives a much stronger agreement without any need for renormalization of the results. In particular, it shows that, as the laser energy increases, the difference among the values of the decay rates pertaining to dotted and continuous lines are relevant. This led us to exclude the evaporation as the main cause of AuNP fragmentation in our experiment.

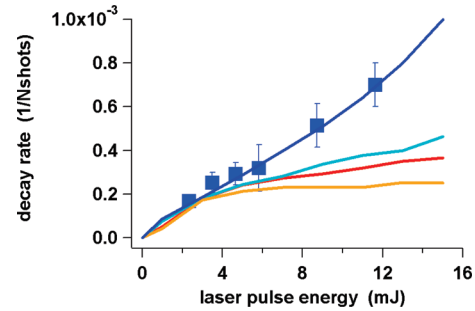

Figure 6. Theoretical dependence of the decay rate versus pulse energy at 355 nm caused by different ionizing processes. Violet line: full model; red line: thermoionic ionization; light-blue line: one-photon ionization; orange line: two-photon ionization. For the convenience of the reader, the experimental data are also reported as references (dots).Volume of bleached suspension 1 cm^3. $W_F = 4.6$ eV.

Let us now elucidate the relative influence of the ionization processes in our conditions. In light of eqs 4, 5, and 7, ionization processes interfere with each other, since they all depend on the total number of atoms contained in a NP. An example of the influence of each ionization process involved in the bleaching at 355 nm is reported in Figure 6. As a reference, we also show the experimental points and the curve from the full model. To make the identification of each term easier, we used the same colors and symbols used in Figure 4 to draw experimental points and theoretical curves from the full model (i.e., violet for 355 nm). Then, we used the red for thermoionic ionization, the light blue for one-photon ionization, and the orange for two-photon ionization. With 532 nm (not shown) we found a similar behavior, apart from some rescaling due to the different laser absorption coefficient, wavelength, and so forth. Figure 6 shows that, especially at low energy, all envisaged processes behave in the same way, and each of them leads to almost the same decay rate. Some differences are found above 4−5 mJ, but they are not sufficiently marked to clearly determine the dominance of one process over another.

Referring to the model, we can give a simple word picture of the time behavior of individual processes responsible for ionization. As the electron temperature increases and hence the electrons populate the gap between Fermi level and continuum, the first process that can be effective is the two-photon ionization for electrons belonging to the energy range within $W_F - 2h\nu$ and $W_F - h\nu$. Making use of eq 5, the corresponding saturation intensities for this process range between 3×10^{10} and 2×10^{11} W/cm^2 for 532 nm and 9×10^{10} and 5×10^{11} W/cm^2 for 355 nm. Our experimental peak intensity range was very similar, that is, in between 2×10^{10} and 3×10^{11} W/cm^2, with both wavelengths. In our intensity range and in the absence of other processes, which can deplete the conduction band before the laser intensity reaches the peak value, two-photon ionization could also cause thorough bleaching in the least favorable case of 355 nm radiation. Nevertheless, as the electron temperature increases during the laser pulse, more and more electrons approach the threshold of the one-photon transition, whose onset is just at $W_F - h\nu$. Then, the saturation intensities drop to the values of 5×10^8 and 1.2×10^9 W/cm^2 for 532 nm and 355 nm, respectively. This means that the one-photon ionization starts to dominate over the two-photon one.

Thermoionic ionization occurs when a significant amount of electrons approach the threshold of the continuum. To be effective, it requires an additional heating, approximately on the order of the photon energy, to be comparable with single photon ionization. Of course, single photon ionization prevails if the intensity is large enough to remove a significant amount of electrons before they move to the continuum. Thus, it not surprising that, in the nanosecond regime and with fluences similar to ours, some authors have found a dominance of thermoionic effect over single photon ionization.[10–12,20] In fact, in the previous nanosecond experiments, the fluence made the electron temperature grow to a value similar to ours, but the intensity was orders of magnitude smaller.

To some extent, the dependence on the laser energy could not be enough to discriminate *a priori* between two- and one-photon ionization. To clarify this point, we assume, for the sake of simplicity, constant values of Fermi energy and work function. The following discussion refers to the evolution during a single laser shot. When a AuNP is cold, i.e., at the beginning of the laser pulse, two-photon ionization, in principle, does not require any electron heating to be effective at both wavelengths, once a reduced work function is assumed, i.e., 4.6 eV (see above). Nevertheless, the laser intensity is still too far from its peak value, i.e., much below the two-photon saturation intensity, to make this process effective. As the laser intensity increases, electrons start to gain energy and move above the Fermi energy. The onsets of single photon ionization are 1.1 and 2.3 eV above the Fermi level for 355 and 532 nm, respectively. Therefore, single photon ionization begins to play a role at a moderate heating for 355 nm pulses, while for 532 nm pulses, it requires a further increase of the electron temperature of about 1.2 eV. It explains why we ascribed the bleaching at 355 nm[21] to a single photon process. Indeed, an electron heating of 1.1 eV is achieved for whatever energy in our range of investigation (see Figures 3 and 4). In contrast, the behavior at 532 nm can be a little trickier and suggests the coexistence and interplay of thermal-assisted one-photon and coherent two-photon ionizations. In fact, since the onset of two-photon ionization is close to the Fermi level, this process works at least until the electron temperature grows up to 2.3 eV, when the single photon becomes effective (see Figure 3). If we assume a grossly linear dependence of electron temperature on pulse energy, it turns out that the single photon ionization can also exhibit a *quasi* quadratic dependence on the laser intensity. This justifies the experimental data that we reported in ref 2. Although we have to conclude that our measurements cannot discriminate a prevailing ionization channel, they are useful to grossly discriminate between evaporation and ionization regimes.

Our model can also explain why, in the experimental conditions of ref 7, evaporation is the dominant effect in the photofragmentation of the AuNPs. As a matter of fact, the much larger size of the AuNPs, about 10 nm, first enhances the lattice temperature by a quadratic increase of the time constant of thermal exchange with the surrounding medium, and hence increases the threshold for Coulomb explosion (eq 9). Indeed, in our experiment, $R_{NP} = 1.75$ nm implies $\tau = 7$ ps and $Q \geq 35$, while the data of ref 7 give $\tau = 230$ ps and $Q \geq 475$.

It is also worth noting that the model makes use of several quantities, such as electron−phonon coupling, electron heat capacity, saturation intensities, and so on, which are known to different degrees of accuracy. Variation for some of them can affect the onset of one effect with respect to the other, but it cannot substantially modify the general scheme.

Furthermore, we assumed that the Fermi distribution function held true even if in a regime of strong nonequilibrium. To our knowledge, the problem was analyzed in detail only in ref 20 by using low values of intensity, when compared to ours. Considering a moderate excursion of the electron temperature, of the order of 1 eV, the authors found a weak modification of the Fermi distribution. Considering our larger range (see Figure 3), modifications could be more significant and shall be addressed in the future. An improvement in this direction seems mandatory to extend the applicability of the model also to femtosecond regimes, where the ultrafast dynamic cannot be neglected.[36,37]

V. Conclusions

We have developed a theoretical model aimed at explaining the mechanism of photofragmentation of AuNPs by picosecond pulses at 532 and 355 nm. It permits a quantitative treatment of the involved phenomena and explains the dependence of the fragmentation on wavelength and pulse energy. The validation with experimental data, some of them already reported in refs 2, 21 and 23, was performed by using AuNPs obtained by picosecond laser ablation in water and stabilized with an organic molecule, PAMAM-G5. PAMAM-G5 plays a key role in the experiments. Its use permits isolation and stabilization of the different products of the photofragmentation and forbids their reaggregation into new particles after the interaction with the laser pulse,[2,21,23] thus making the monitoring of the bleaching process clearer and easier. We found that evaporation of the nanoparticles does not play a relevant role in our experimental conditions and that photofragmentation is due to the interplay of thermoionic electron emission and photon-assisted ionization.

We stress that our model constitutes an *ab initio* calculation, which starts from the experimental parameters related to the laser, the focusing geometry, and the nature of the suspension. In this sense, it is also able to justify the experimental findings obtained by other authors in picosecond and nanosecond regimes, which were in apparent contrast with ours. We think that, in its present form, the model can represent a useful tool to approach the laser−AuNP interaction in different conditions and, particularly, in the regime of nanosecond and picosecond pulses.

Acknowledgment. Funding from the Italian Project PRIN2007 "Nanostrutture plasmoniche metallo-organico per sensoristica" is acknowledged.

References and Notes

(1) Jain, P. K.; Quian, W.; El-Sayed, M. A. *J. Phys. Chem. B* **2006**, *110*, 136. Jain, P. K.; El-Sayed, I. H.; El-Sayed, M. A. *NanoToday* **2007**, *2*, 18, and references therein.
(2) Giusti, A.; Giorgetti, E.; Laza, S.; Marsili, P.; Giammanco, F. *J. Phys. Chem. C* **2007**, *111*, 14984.
(3) Kamat, P. V.; Flumiani, M.; Hartland, G. V. *J. Phys. Chem. B* **1998**, *102*, 3123.
(4) Fujiwara, H.; Yanagida, S.; Kamat, V. P. *J. Phys. Chem. B* **1999**, *103*, 2589.
(5) Takami, A.; Kurita, H.; Koda, S. *J. Phys. Chem. B* **1999**, *103*, 1226.
(6) Mafune', F.; Kohno, J.; Takeda, Y.; Kondow, T. *J. Phys. Chem. B* **2000**, *104*, 9111.
(7) Inasawa, S.; Sugiyama, M.; Yamaguchi, Y. *J. Phys. Chem. B* **2005**, *109*, 9404.
(8) Peng, Z.; Walther, T.; Kleinermanns, K. *J. Phys. Chem. B* **2005**, *109*, 15735.
(9) Kawasaki, M.; Masuda, K. *J. Phys. Chem. B* **2005**, *109*, 9379.
(10) Yamada, K.; Tokumoto, Y.; Nagata, T.; Mafune', F. *J. Phys. Chem. B* **2006**, *110*, 11751.
(11) Yamada, K.; Miyajiama, K.; Mafune', F. *J. Phys. Chem. B* **2007**, *111*, 11246.

(12) Shoji, M.; Miyajima, K.; Mafunè, F. *J. Phys. Chem. C* **2008**, *112*, 1929.
(13) Ahamadi, T. S.; Logunov, S. L.; El-Sayed, *J. Phys. Chem.* **1996**, *100*, 8053.
(14) Inasawa, S.; Sugiyama, M.; Noda, S.; Yamaguchi, Y. *J. Phys. Chem. B* **2006**, *110*, 3114.
(15) Buffat, Ph.; Borel, J.-P. *Phys. Rev. A* **1776**, *13*, 2287.
(16) Couchman, P. R.; Jesser, W. A. *Nature* **1977**, *269*, 481.
(17) Hu, M.; Hartland, G. V. *J. Phys. Chem. B* **2002**, *106*, 7029.
(18) Plech, A.; Kotaidis, V.; Gresillon, S.; Dahmen, C.; von Plessen, G. *Phys. Rev. B* **2004**, *70*, 195423.
(19) Kotaidis, V.; Dahmen, C.; von Plessen, G.; Springer, F.; Plech, A. *J. Chem. Phys.* **2006**, *124*, 184702.
(20) Grua, P.; Morreeuw, J. P.; Bercegol, H.; Jonusauskas, G.; Vallèe, F. *Phys. Rev. B* **2003**, *68*, 35424.
(21) Giorgetti, E.; Giusti, A.; Giammanco, F.; Marsili, P. *Opt. Spectrosc.* **2009**, *107*, 505.
(22) Pal, K. *Talanta* **1998**, *46*, 583.
(23) Giorgetti, E.; Giusti, A.; Giammanco, F.; Marsili, P.; Laza, S. *Molecules* **2009**, *14*, 3731.
(24) Saunders, W. A. *Phys. Rev. A* **1992**, *46*, 7028.
(25) Knecht, M. R.; Gracia-Martinez, J. C.; Crooks, R. M. *Langmuir* **2005**, *21*, 11981.
(26) *CRC Handbook of Chemistry and Physics*; CRC Press: London, 1998/99.
(27) Kreibig U.; Vollmer M., *Optical Properties of Metal Clusters*; Springer Verlag: Berlin, 1995.
(28) Muto, H.; Yamada, K.; Miyajiama, K.; Mafune', F. *J. Phys. Chem. C* **2007**, *111*, 17221.
(29) Werner, D.; Hashimoto, S.; Tomita, T.; Matsuo, S.; Makita, Y. *J. Phys. Chem. C* **2008**, *112*, 16801.
(30) Lin, Z.; Zhigilei, L. V. *Phys. Rev. B* **2008**, *77*, 075133http://www.faculty.virginia.edu/CompMat/electron-phonon-coupling/.
(31) Sadaiyandi, K. *Mater. Chem. Phys.* **2009**, *115*, 703.
(32) Hache, F.; Ricard, D.; Flytzanis, C.; Kreibig, U. *Appl. Phys. A: Mater. Sci. Process.* **1998**, *47*, 347.
(33) Chang, B.; Bolton, P. R.; Fittinghoff, D. N. *Phys. Rev. A* **1993**, *47*, 4193.
(34) Jackson D. *Classical Electrodynamics*; John Wiley & Sons: New York, 1962; Chapter 2.
(35) Halas, S.; Durakiewicz, T. *J. Phys.: Condens. Matter* **1998**, *10*, 10815.
(36) Lugovsky, A.; Bray, I. *Phys. Rev. B* **1999**, *60*, 3279.
(37) Voisin, C.; Del Fatti, N.; Christofilos, D.; Vallée, F. *J. Phys. Chem. B* **2001**, *105*, 2264.

JP908964T